Nanoscale

Accepted Manuscript

This article can be cited before page numbers have been issued, to do this please use: L. Giraud, O. Marsan, E. Dague, M. Ben-Neji, C. Cougoule, E. Meunier, S. Soueid, A. M. Galibert, A. Tourrette and E. Flahaut, *Nanoscale*, 2024, DOI: 10.1039/D4NR02810D.

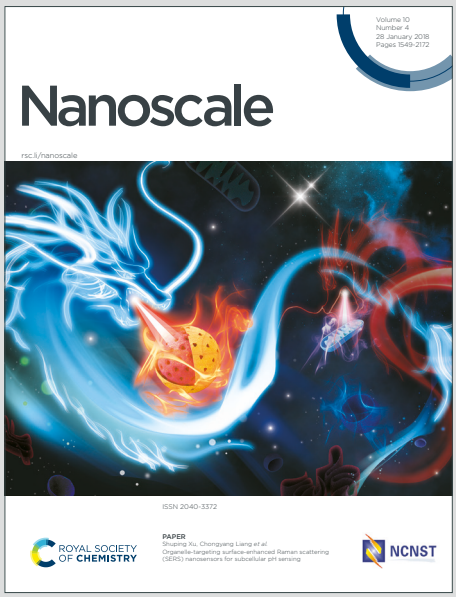

ROYAL SOCIETY OF CHEMISTRY

rsc.li/nanoscale

View Article Online
DOI: 10.1039/D4NR02810D

Surface-anchored Carbon Nanomaterials for antimicrobial surfaces

L. Giraud[1], O. Marsan[1], E. Dague[2], M. Ben-Neji[3], C. Cougoule[3], E. Meunier[3], S. Soueid[1], A. M. Galibert[1], A. Tourrette[1*] and E. Flahaut[1*]

[1]. CIRIMAT, Université Toulouse 3 Paul Sabatier, CNRS, INP Toulouse, Toulouse, France

[2]. LAAS-CNRS, Université de Toulouse, CNRS, Toulouse, France

[3]. Institut de Pharmacologie et de Biologie Structurale (IPBS), Université de Toulouse, CNRS, Université Toulouse III - Paul Sabatier (UT3), Toulouse, France

Corresponding Authors

A. Tourrette*, CIRIMAT, Université Toulouse 3 Paul Sabatier, CNRS, INP Toulouse, Toulouse, France
ORCID: 0000-0003-1107-2176

E. Flahaut*, CIRIMAT, Université Toulouse 3 Paul Sabatier, CNRS, INP Toulouse, Toulouse, France
ORCID: 0000-0001-8344-6902

Abstract

Carbon nanomaterials (CNM) are known for their antimicrobial (antibacterial, antiviral) activity when dispersed in a liquid, but whether this can be transferred to the surface of common materials has rarely been investigated. We have compared two typical CNM (double-walled carbon nanotubes and few-layer graphene) in their non-oxidised and oxidised forms in terms of their antibacterial (*Pseudomonas aeruginosa*, *Staphylococcus aureus*) and antiviral (SARS-CoV2) activity after anchoring them on the surface of silicone. We propose a very simple and effective protocol using air-brush spray deposition method to entrap CNM on the surface

View Article Online
DOI: 10.1039/D4NR02810D

of two different silicone materials and demonstrate that the nanomaterials are anchored within the polymer while still in contact with bacteria. We also investigated their antiviral activity against SARS-COV2 after deposition on standard surgical respiratory masks. Our results show that while suspensions of double-walled carbon nanotubes had a moderate effect on *P. aeruginosa*, this was not transferred after anchoring them to the surface of silicone. On the contrary, graphene oxide showed a very strong antibacterial effect on *P. aeruginosa* and oxidised double-walled carbon nanotubes on *S. aureus* only when anchored to the surface. No significant antiviral activity was observed. This work paves the way for new antibacterial surfaces based on CNM.

Keywords

Carbon nanomaterials; carbon nanotubes; graphene; graphene oxide; antibacterial; antiviral; *Pseudomonas aeruginosa*; *Staphylococcus aureus*; COVID-19

1. INTRODUCTION

Microbial infections, system contaminations and biodegradation due to biofilm formation have become major issues and present serious health and economic consequences [1]. These issues concern many areas, from the food industry to the medical [2] and environmental [3] fields. Bacteria produce biofilms on materials facing environmentally challenging conditions such as implantable medical devices or materials immersed in aquatic media. Biofilms, which can be considered as structured agglomerates of microorganisms contained in a self-produced matrix, are often very difficult to remove once established. Bacterial resistance to antibiotics is also widely increasing. Therefore, it is essential to develop antimicrobial materials, with other mechanisms of action, able to inhibit microbial proliferation. The literature provides many different solutions to process a surface to fight against microbes. This can be obtained by killing or degrading the pathogens at the surface, or only by preventing biofilm formation, or more generally speaking, adhesion of pathogens,

View Article Online
DOI: 10.1039/D4NR02810D

while not necessarily destroying them [4]. In most cases, antimicrobial substances (drugs, toxic metal ions – sometimes released from nanoparticles, *etc*. [5–8]) are released, which also means that this action is necessarily limited in time. Durability can thus only be achieved in the absence of release.

We propose here that carbon nanomaterials, which have attracted attention for their antimicrobial properties when used in suspension [9,10], may still be a good option to achieve durable antimicrobial surfaces after deposition. Carbon nanomaterials (CNM) represent a specific category of nanoparticles that are widely known thanks to their exceptional properties [11]. In particular, the fact that they are not soluble and exhibit a very strong chemical resistance ensures a durable action over time. Their antimicrobial properties are described in the literature, and the most widely mentioned carbon nanomaterials (CNM) are graphene, carbon nanotubes and their oxidized forms [12]. Most studies focus on the antibacterial activity of CNM in suspension and the mainly reported mechanisms are oxidative stress and physical damage that are induced by the nanoparticles on cells. This topic is closely related to the potential toxicity of most CNM. For the sake of durability and to avoid potential toxicity in case of release in the environment, it is of paramount importance to ensure that CNM cannot leave from antimicrobial materials. There is thus a growing interest in antimicrobial composites based on the inclusion of CNM in different matrices [12]. This increasing use of carbon nanoparticles may be related to the availability of these materials, CNM becoming more and more affordable with the improvement of their synthesis methods. For economic reasons, it is certainly better to localise antimicrobial nanomaterials only at the surface of materials to be protected, because the antimicrobial activity can be expressed only in case of contact. However, it may still be interesting to include the nanomaterials not only at the surface but also within a short depth, to regenerate an antimicrobial surface in case, for

View Article Online
DOI: 10.1039/D4NR02810D

instance, of abrasion. Most studies in the literature deal with composites containing carbon nanomaterials embedded in a matrix, as this is the easiest way to incorporate CNM at the surface. However, the majority of embedded CNM are of no use as they are inaccessible. Here we propose a very simple method allowing the development of materials with carbon nanoparticles emerging from the surface while being anchored onto the matrix. This is to the best of our knowledge the first claim of such a strategy.

Ideally, CNM should be deposited directly at the surface of a material while ensuring a proper anchorage to prevent their release, while maintaining the possibility of direct contact with pathogens. The objective of this work is thus to propose a method to develop antimicrobial materials based on CNM in a "*safer by design*" approach. The challenge is to succeed in blocking CNM on the surface of a polymer in such a way as to avoid a loss of efficiency over time, thus overcoming any toxicity associated with release. Focusing on the interface between CNM and microorganisms also aims to decrease the required amount of CNM by limiting their incorporation only at the surface and not in the bulk of the material where microbes do not have access. Very few methods allowing nanoparticles to emerge from the matrix are reported in the literature [12]. In this work, we have selected airbrush deposition because of its availability, very simple use, and novelty in this application.

We have compared the CNM mostly reported in the literature [12] for their antimicrobial activity: raw and oxidized carbon nanotubes, few-layer graphene (FLG) and graphene oxide (GO). We have selected double-walled carbon nanotubes (raw DWCNT and DWCNT Ox) as a representative model for CNTs in general as they lie at the interface between single- and multi-walled carbon nanotubes. We have selected silicone as the material to which these antimicrobial properties should be transferred, mainly because this polymer is often used for medical devices intended for medium-term implantation, where microbial

View Article Online
DOI: 10.1039/D4NR02810D

proliferation is thus likely to become a serious issue if it occurs. This study aims to show that airbrush deposition of water-based suspensions can be used to anchor CNM, and then compare each CNM activity towards two models of nosocomial bacteria (*P. aeruginosa*, Gram-negative, and *S. aureus*, Gram-positive) in suspension or after anchoring at the surface of silicone. To widen our study, we also aimed to compare different kinds of silicone, one of them being of medical grade. Finally, as relatively little information relating to the antiviral activity of carbon nanoparticles is available and in the context of the COVID-19 pandemic, we also investigated the antiviral activity of the same CNM against SARS-COV2. This was done by applying the same airbrush deposition method on surgical FFP1 respiratory mask tissue followed by a comparison of the antiviral activity with a commercial graphene mask. There is a growing interest in the study of the antiviral properties of CNM [23,24]. This study also compares the antiviral activity of masks spray-coated with four different kinds of carbon nanomaterials.

Briefly, our main objective is to integrate CNM only at the surface while anchoring them to avoid unwanted release. This safer-by-design strategy which can be achieved by a simple airbrush spray deposition method as reported here, aims to propose engineering solutions for the responsible use of nanomaterials. This work also paves the way towards more durable antimicrobial surfaces, with no loss of activity with time, and without the need to release toxic substances (molecules, ions).

2. EXPERIMENTAL SECTION

2.1 Carbon nanomaterials (CNM): We used DWCNT which we consider as a general model for CNT. The synthesis was described elsewhere [27]. Oxidized DWCNT (DWCNT Ox) were prepared by refluxing DWCNT in a HNO_3 (3M) solution at 130°C for 24h. After cooling down to

View Article Online
DOI: 10.1039/D4NR02810D

room temperature, the oxidized nanotubes were washed with deionized water (0.45 µm polypropylene filtration membrane) until neutrality. Graphene oxide (GO) was synthesised by a modified Hummers method [28]. 30 mL of H_2SO_4 (98 wt.%), 0.5 g of $NaNO_3$ and 3 g of $KMnO_4$ were added to 0.5 g of graphite into a flask and stirred 1h at room temperature to obtain a homogeneous suspension. The mixture was then placed in a laboratory oven at 45°C for two days. The mixture was degassed, and 40 mL of deionized water was added under stirring. After 1 h, another 50 mL of deionized water was added to the mixture under stirring, then 3 g of H_2O_2 was slowly added, and 50 mL of deionized water was added again. After 2 h at room temperature, the sample was centrifuged at 4 500 rpm for 10 min. The supernatant was removed and NaOH was added to the pellet until a pH of 8.5 was reached. Ultrasonic treatment was used to further exfoliate the GO nanosheets. FLG was supplied by BeDimensional (Italy) as a powder containing sodium deoxycholate, which was removed by thorough washing with deionised water (completion of the washing was controlled by TGA). DWCNT Ox and GO are rather stable in water, as opposed to raw DWCNT and FLG. Ultra-low viscosity carboxymethylcellulose (CMC, Fluka 21901) was added to the aqueous suspensions (deionised water) of FLG and DWCNT, at the same weight ratio as the nanoparticles (1 $mg.mL^{-1}$), to ensure a stable dispersion and stabilise the suspension. Suspensions were bath sonicated (Elmasonic S30H, 280W, 50/60 Hz)) for 30 minutes, followed by probe sonication (VibraCell 75042, 500W, 20 kHz, tip diameter: 13mm) for 1 minute (30%, cycles of 3 sec. on, 3 sec. off).

2.2 Silicone: We used in this work two different silicones. SYLGARD184 (S184) bi-component silicone elastomer with a ratio of 1:10 was purchased from Dow Corning. Its ideal polymerization conditions should not exceed 60°C. MED4729 (MED) bi-component biomedical silicon elastomer with a ratio of 1:1 was supplied by Nusil. Mixed components were degassed

View Article Online
DOI: 10.1039/D4NR02810D

for 30 min in a vacuum, then 0.6 g was poured into each well of a 12-well polystyrene culture plate. The spray coating of CNM suspensions was performed on fully polymerised silicone.

2.3 Surgical respiratory mask: For antiviral properties assessment, standard polypropylene surgical type surgical class respiratory mask (Securimed), as well as a commercial FFP2 graphene mask (Shandong Shengquan New Materials Co. Ltd. Biomass graphene) were used.

2.4 Spray deposition: Carbon nanomaterials (CNM) were deposited either on silicone or on a commercial surgical respiratory mask (FFP1, polypropylene) using an airbrush. CNM were first dispersed in deionised water at a concentration of 1 mg.mL^{-1}. In the case of the non-oxidized CNM (DWCNT, FLG), carboxymethylcellulose (Fluka 21901) was added at the same concentration of 1 mg.mL^{-1}. Before airbrush deposition, the suspension of CNM was bath-sonicated for 2 minutes to ensure the proper dispersion of the CNM. A multi-well plate (filled with silicone or surgical mask) was fixed on a stand. An air model airbrush (nozzle diameter of 0.3 mm, supplied at 2 bars with compressed air (AS18-2 airbrush compressor)) was used to spray the dispersion 20 cm away from the target 2 mL of suspension were sprayed with regular and repeated movements over the whole surface of the plate to ensure a homogeneous deposit. Plates containing deposits on silicone were cleaned in an ultrasonic bath for 2 minutes to remove the nanoparticles not properly entrapped at the surface. In the case of CNM deposited on mask samples, we did not apply the cleaning step.

2.5 Samples characterisation: Scanning Electron Microscopy (SEM) observations were performed using a FEG FEI QUANTA 250 SEM operated at 10 kV. Drops of aqueous suspensions of CNM were deposited on SEM support and observations were performed directly after drying in an oven. Silver lacquer and 5 nm platinum metallization were applied to silicone samples prior to observation. Mask samples were observed under partial vacuum (90 Pa). Transmission Electron Microscopy (TEM) observations were performed using a JEOL JEM 1400

View Article Online
DOI: 10.1039/D4NR02810D

ORIUS TEM operated at 120 kV. Atomic Force Microscopy (AFM) experiments were performed using Nanowizard III (JPK instruments Germany) and MLCT cantilevers (Brucker) in contact mode at room temperature. The probe used was systematically calibrated, the spring constants were measured by the thermal noise method and were between 0.591 and 0.796 N/m. The measures were carried out in Quantitative Imaging mode on an area of 10 x 10 µm², with a resolution of 256 x 256 pixels, a maximum applied force of 2 nN, a Z length of 0.28 µm and a speed of 30 $\mu m.s^{-1}$ [29]. Measures on materials were performed in deionised water; a drop was placed under the cantilever on the sample surface. The data were analysed using the JPK Data Processing software (version 6) to produce topographical maps, adhesion maps and rigidity maps. In QI mode, force curves are recorded on each pixel and height, adhesion and rigidity can be extracted from the force curves as explained elsewhere [29, 30]. Raman analyses were performed with a Jobin Yvon Labram HR800 RAMAN confocal microscope. The samples were exposed to continuous laser radiation provided by a He laser at 633 nm with a power of 8 mW. Attenuation filters, lowering the laser power by 10, were used to avoid any degradation of the materials. The samples were placed under a BX 41 Olympus microscope and focused under a x100 objective with a numerical aperture of 0.90 which gave the system a lateral resolution of 0.858 µm (1.22 x λ / O.N) and an axial resolution of 3.12 µm (4 x λ / $O.N^2$). The maps were produced using a motorized XYZ table with an accuracy of 0.1 µm and a measurement step of 3 µm on the X and Y axis and 2 µm in Z. The equipment's frequency was calibrated using the order 1 line of silicon at 520.7 cm^{-1} with an accuracy of ± 1cm^{-1}. Each point spectrum was acquired using a 600 gr/mm grating with a 1 cm^{-1} spectral resolution and collected with a quantum well detector cooled to -60°C by the double Peltier effect (CCD Synapse). Each map spectrum was acquired with a time of 30 seconds and 1 accumulation. Data processing was performed using Labspec6 software. The X-ray photoelectron

View Article Online
DOI: 10.1039/D4NR02810D

spectrometry (XPS) analysis was performed on a Kratos Axis Ultra (Kratos Analytical, U.K.). An adhesive copper tape was used to fix the samples. The spectrometer is equipped with a monochromatic Al Kα source (1486.6 eV). All spectra were recorded at a 90° take-off angle, with an analysed area of about 0.7 × 0.3 mm. Survey spectra were acquired with 1.0 eV step and 160 eV analyser pass energy. The high-resolution regions were acquired with 0.1 eV step (0.05 eV for O 1s and C 1s) and 20 eV pass energy. A neutralizer was used to perform the recording to compensate for the charge effects. Curves were fitted using a Gaussian/Lorentzian (70/30) peak shape after Shirley's background subtraction and using CasaXPS software. The carbon C 1s was calibrated at 284.8 ev for C-C and C-H bonds. Specific surface area (SSA) was measured using a ASAP 2010 M (Micromeritics) after degassing at 80°C for 20 h, in vacuum.

2.6 Microbial strains and media: Nunclon Delta surface 6-12-24 and 96-well plates (Thermo Scientific), Luria Broth LB liquid and LB agar medium Fisher Scientific were used. Bacterial strains Gram-negative *Pseudomonas aeruginosa* (strain PAO1, ATCC) and Gram-positive *Staphylococcus aureus* (strain USA-300, ATCC) provided by Institute of Pharmacology and Structural Biology (IPBS-Toulouse) were used for antibacterial assays. All described experiments involving *Pseudomonas aeruginosa* and *Staphylococcus aureus* have been entirely performed and processed in a Biosafety Level 2 (BSL-2) facility. The bacteria were preserved in glycerol stock solution at -70°C. Bacteria were grown overnight in LB medium at 37°C and 160 rpm. Bacteria were sub-cultured the next day by dilution overnight culture 1/50 and grown until reaching an optical density (OD) at 600 nm of 0.5-1. Afterwards, the cells were harvested by centrifugation at 5000 rpm for 10 min and washed 3 times in phosphate-buffered saline (PBS; pH 7.3) medium. The concentration of bacterial suspensions in PBS was finally adjusted to the target concentration. Viral strain SARS-CoV-2 (BetaCoV/France/IDF0372/2020

View Article Online
DOI: 10.1039/D4NR02810D

isolate kindly supplied by Sylvie van der Werf and the National Reference Centre for Respiratory Viruses hosted by Institute Pasteur (Paris, France)) was used for antiviral assays. All described experiments involving SARS-CoV-2 infections have been entirely performed and processed in a Biosafety Level 3 (BSL-3) facility.

2.7 Antibacterial tests: Colony forming units assay: The concentration of *P. aeruginosa* and *S. aureus* was adjusted to 10^7 and 10^8 bact.mL^{-1} respectively, to first evaluate the antibacterial activity of CNM free in suspension. These tests were performed with the incubation of 250 µL of bacterial suspension with 250 µL of CNM suspended in PBS at a concentration of 150 µg.mL^{-1}, at 37°C. Only 8 wells in the centre of a 24-wells culture plate were used, the other ones were filled with PBS to avoid evaporation. The plates were covered with aluminium foil and incubated for 24 h at 37°C under continuous stirring (160 rpm). Incubated suspensions were then diluted in PBS (1/20^4 and 1/20^3 for *P. aeruginosa* and *S. aureus* suspensions, resp.), and 100 µL of adequate dilution were spread in the wells of 6-well culture plates, each filled with 4 mL of LB agar nutritive medium. Three marbles were placed in each well and plates were shaken to spread bacteria. Next, the plates were flipped upside down, covered with aluminium foil and incubated overnight at 37°C before finally passing to colony counting. The evaluation of the antibacterial activity of CNM deposited on silicone was performed with the incubation of 75 µL of bacterial suspension on the samples. The concentration of *P. aeruginosa* and *S. aureus* suspensions used were 10^5 bact.mL^{-1} and 10^6 bact.mL^{-1}, resp. Only the middle wells of 12-well culture plates were used, the other ones were filled with PBS to avoid evaporation. The plates were covered with aluminium foil and incubated for 24 h at room temperature. Then incubated suspensions were diluted in PBS with a factor of 1/20^2, and 100 µL of the dilutions were spread on the wells of a 6-well culture plate, each filled with 4 mL of LB agar nutritive medium. Three marbles were disposed of in every well and plates were

View Article Online
DOI: 10.1039/D4NR02810D

shaken to spread bacteria in the wells. Next, the plates were flipped upside down, covered with aluminium foil and incubated overnight at 37°C before finally processing for colony counting. Counted colonies were compared with those on control plates to evaluate the antibacterial effect. The control of the test on CNM suspension was PBS without CNM, and the control of the tests on spray-deposited CNM was the silicone material alone. Data are expressed as the number of cells.mL^{-1} and were analysed using ANOVA variance for calculation of statistical significance between samples. Data were analysed using one-way ANOVA with multiple corrections statistical test. A probability value p of $p<0.05$ was considered statistically significant. Each tested condition was prepared in triplicate and repeated in three independent experiments.

2.8 Tissue Culture Infective Dose 50 $TCID_{50}$ assay: First, to determine the optimal dose of virus to be used in the assay, three doses of SARS-CoV-2 (10^3, 10^6, 10^7 PFU) were incubated in 500 µl of serum-free DMEM culture medium and the number of infectious viral particles was measured at 6 h, 24 h and 48 h, by TCID50 assay. Mask samples (Fig. S5-S7) were cut to be adapted to the size of 24-well plate and fixed at the bottom using carbon tape to ensure the correct deposition of the viral solution on its surface. First, 10^6 infectious particles of SARS-CoV-2 in 500 µl of serum-free DMEM culture medium were deposited on the tested material for 24 h in monoplicates. A well containing the untreated material was used to test the intrinsic activity of the material. The antiviral activity of the CNM sprayed on silicone or mask substrate (either sprayed in the same conditions on a classical FFP1 surgical mask or using a commercial graphene mask) was evaluated with the Tissue Culture Infective Dose 50 (TCID50) assay in quadruplets as previously described [31], which determines the quantity of virus necessary to induce cytopathic effects on half of the Vero E6 cells. These results are expressed in $TCID_{50}$.mL^{-1} value and the student's T-test (T. Test) was applied with a bilateral distribution

View Article Online
DOI: 10.1039/D4NR02810D

to statistically evaluate the viricidal activity of the samples. A probability of p-value <0.05 was considered statistically significant. At least, three independent experiments were performed.

2.9 Cytotoxicity assay: Vero E6 cells were incubated with the different suspensions of CNM between 1.25 and 150 µg.mL^{-1} (serial dilutions of a mother suspension at 300 µg.mL^{-1}) in a 96-well plate in quadruplets. After 72 h, cell death was evaluated by measuring the release of lactate dehydrogenase (LDH) into the culture medium according to manufacturer instructions (Takara).

3. RESULTS AND DISCUSSION

3.1 Carbon nanomaterials

SEM observations of raw DWCNT Figure 1 (a) reveal large clusters (up to 5 microns) from which structures emerge that likely correspond to bundles of nanotubes, based on this scale. The TEM observation Figure 1 (b) also evidence the presence of bundles of carbon nanotubes (diameter of a few tens of nm [27]), although individual nanotubes are also visible. Clusters of very different shapes (containing a mixture of disorganized carbon and carbon nanotubes) are observed, as well as catalyst nanoparticles that appear as very high-contrast spots [32]. Previous work has shown that the disorganized carbon clusters come from the catalytic decomposition of methane on the magnesia - which constitutes the support on which the catalytic Co:Mo nanoparticles are generated [18]. Other work has demonstrated that metal Co:Mo nanoparticles are tightly encapsulated in concentric carbon shells (carbon onions), and therefore fully inaccessible [33].

SEM and TEM observations of FLG highlight its 2D nature in Figure 1 (c, d). The presence of superimposed sheets is clearly visible and the transparency to electrons confirm the "few-

View Article Online
DOI: 10.1039/D4NR02810D

layer" nature. The lateral dimensions of the nanoparticles generally ranged between 1 and 5 microns (with a few larger particles up to 10 microns).

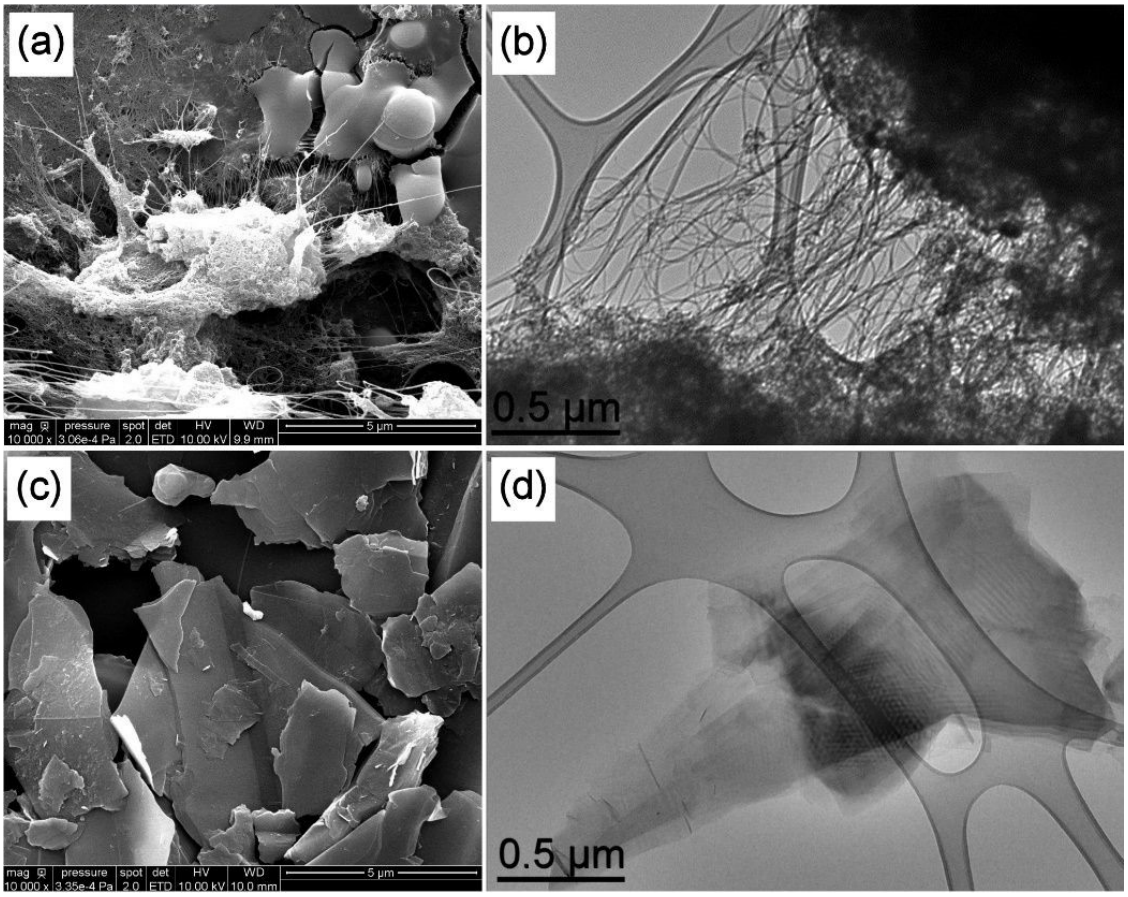

Figure 1: SEM (scale bar 5 µm) and TEM (scale bar 0.5 µm) observations of raw DWCNT (a, b) and FLG (c, d).

Oxidized DWCNT appear more compact than raw DWCNT on the SEM image shown in Figure 2(a); this is likely to come from their more hydrophilic nature. The same observations as for raw DWCNT may be made on the TEM image Figure 2(b) where large clusters and bundles of carbon nanotubes are visible. The SEM observation of GO nanoparticles highlights its 2D nature, with layers clearly visible (Figure 2 (c)). As GO nanoparticles are much less conductive than FLG, a metallisation was required for the SEM observation and is visible in Figure 2(c). Even at this low magnification, TEM observations suggest that GO is much more defective than FLG with the absence of moiré patterns, and a "crumpled" morphology (Figure 2(d)).

View Article Online
DOI: 10.1039/D4NR02810D

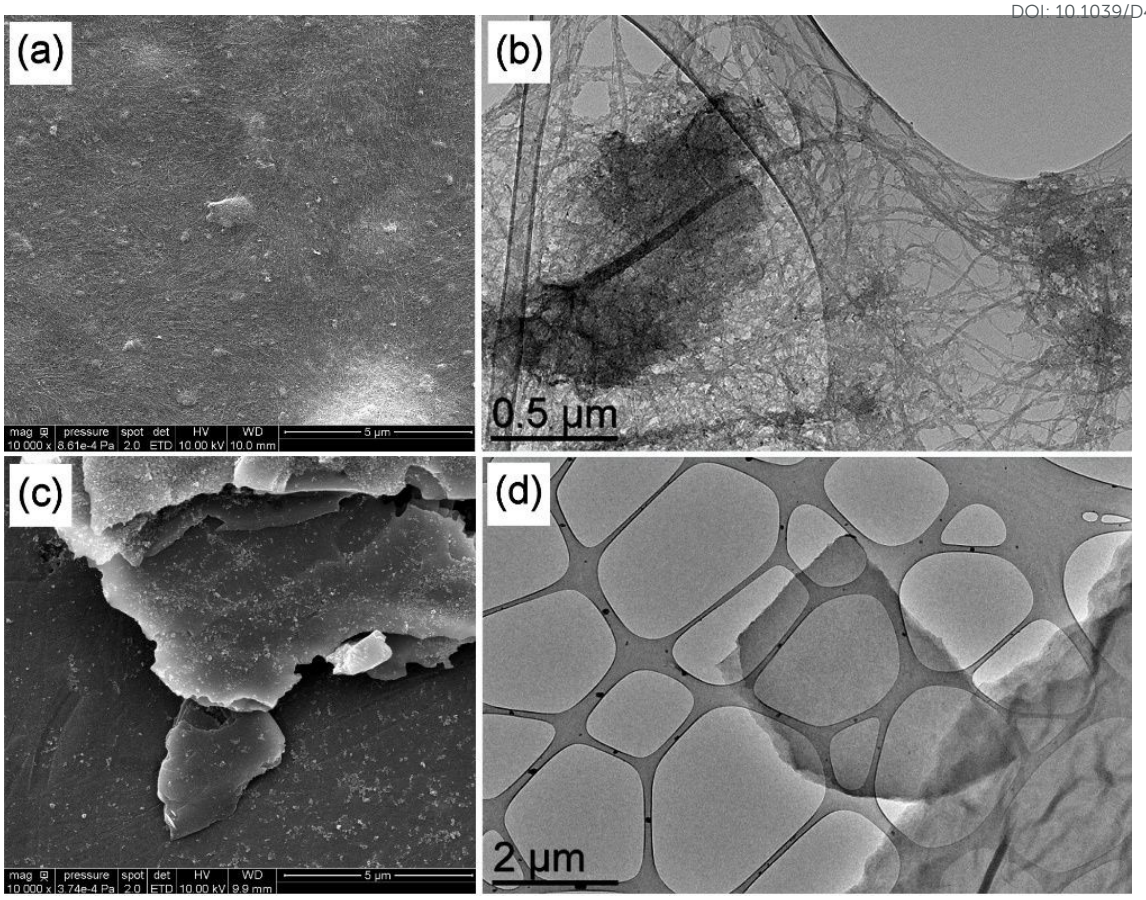

Figure 2: SEM (scale bar 1 µm) and TEM (scale bar 0.5 µm) observations of oxidized DWCNT (a, b) and GO (c, d).

D band around 1330 cm^{-1} and G band at 1590 cm^{-1} are visible for all CNM Raman spectra (Figure 3). D band is generally associated to defects in carbon-based materials and G peak is characteristic of sp^2 carbon, the expected main hybridisation in such carbon nanomaterials. The ID/IG ratio (intensity ratio between D and G bands) of raw DWCNT is 0.26, which reflects a relatively good structural quality of these nanoparticles (Figure 3 (a)). The ID/IG ratio increases to 0.37 in the case of DWCNT Ox, which highlights the expected alteration of the hexagonal carbon network in these nanotubes following the oxidation step (Figure 3 (c)). RBM peaks (Radial Breathing Modes, very sensitive to the diameter of the carbon nanotubes, between 150 and 300 cm^{-1}) can be observed for both samples, as well as the G' peak at *ca.* 2640 cm^{-1}. We may note the attenuation of the RBM peaks in the case of oxidized

View Article Online
DOI: 10.1039/D4NR02810D

DWCNT, which is probably linked to the damage suffered. The ID/IG ratio is 0.10 for the FLG, which reflects very good structural quality, as can be expected from a sample prepared by graphite exfoliation (Figure 3 (b)). In the case of GO, the ID/G ratio is 1.27 (Figure 3 (d)). This very high value denotes the very high structural disorder of this sample, as seen on the TEM image (Figure 2 (d)). Elemental analysis (content in carbon and oxygen) was obtained by XPS (Figures S1, S2). Characterisation data of the 4 CNM are summarized in Table 1.

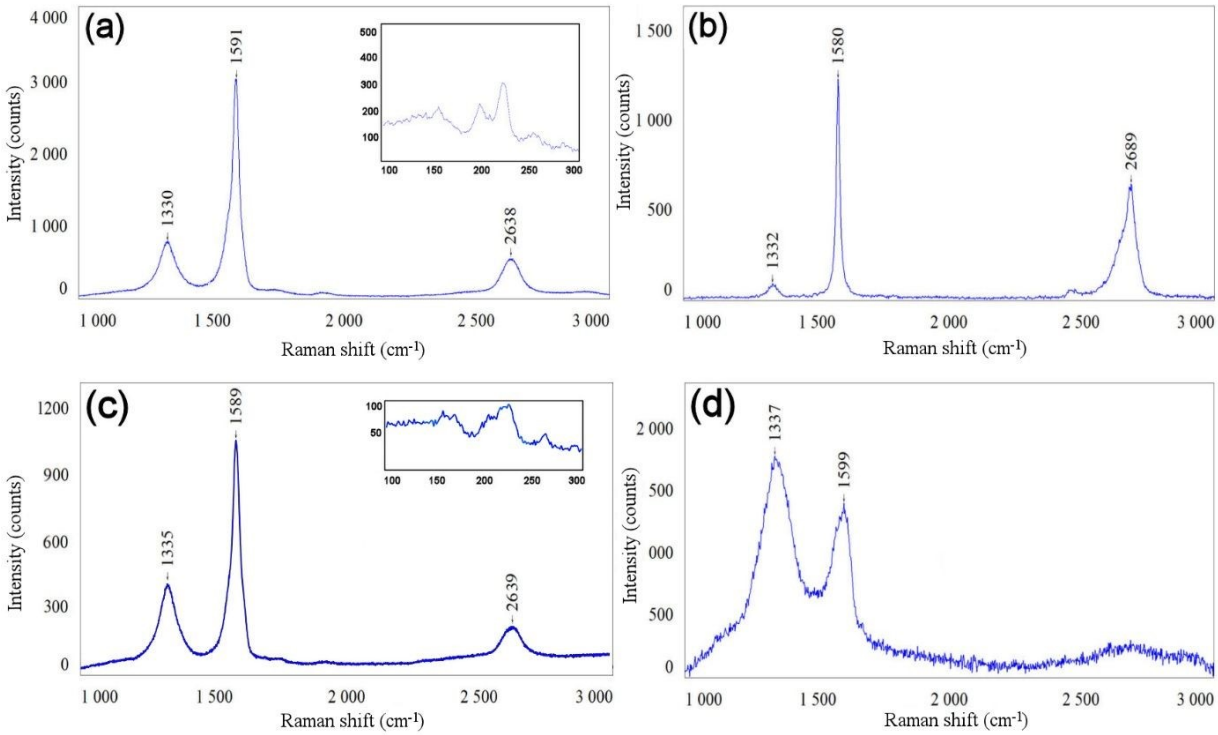

Figure 3: Raman spectra of raw DWCNT (a); FLG (b); DWCNT Ox (c); GO (d). Inserts in (a) and (c) correspond to RBM peaks. λ= 633 nm.

Table 1: Main physico-chemical characteristics of the used carbon nanomaterials; Carbon mass percentage and oxygen mass percentage of raw DWCNT, oxidized DWCNT, FLG and GO samples from XPS analysis; size; Raman ID/IG ratio and Specific Surface Area (SSA)

	DWCNT	DWCNT Ox	FLG	GO
C wt.%	93	84	95	66
O wt. %	3	15	5	29
Other elements wt.%	4 (Co, Mo)	<1 (Co, Mo)	-	Traces (Mn, S)
Size	Diameter: 1-3 nm Length: 1-10 µm (Bundles: diameter < 50 nm; length up to 100 µm)	Identical to DWCNT (unmodified)	Lateral size: mainly between 1 and 5 µm. Thickness: estimated < 10 layers by HRTEM	Lateral size: mainly between 1 and 5 µm. Thickness: estimated < 10 layers by HRTEM

View Article Online
DOI: 10.1039/D4NR02810D

I_D/I_G	0.26	0.37	0.10	1.27
SSA (m^2/g)	980	504	3-4	8

3.2 CNM after airbrush deposition on silicone

SEM observations (Figure S3) of the silicone materials after airbrush deposition of a control CMC solution in deionised water at the same concentration used to stabilise non-oxidised CNM (DWCNT, FLG) clearly evidence the presence of CMC particles at the surface, but also their full removal following the 2-minute ultrasound treatment performed on samples after airbrush deposition (flat and clean surface). Low-magnification SEM observations were performed on the samples, and numerous clusters of CNM were observed on the surface and appeared to be homogeneously dispersed (Figure S4). The modulation of airbrush flowrate only increased spot size (Fig. S4b), but had no influence on the presence of the deposit at the surface of silicone following bath sonication cleaning. The pressure of the equipment used in this work could not be modulated. The resolution of SEM is not enough to distinguish individual CNM particles and only bundles / agglomerates may be observed. The presence of the former may thus not be excluded.

View Article Online
DOI: 10.1039/D4NR02810D

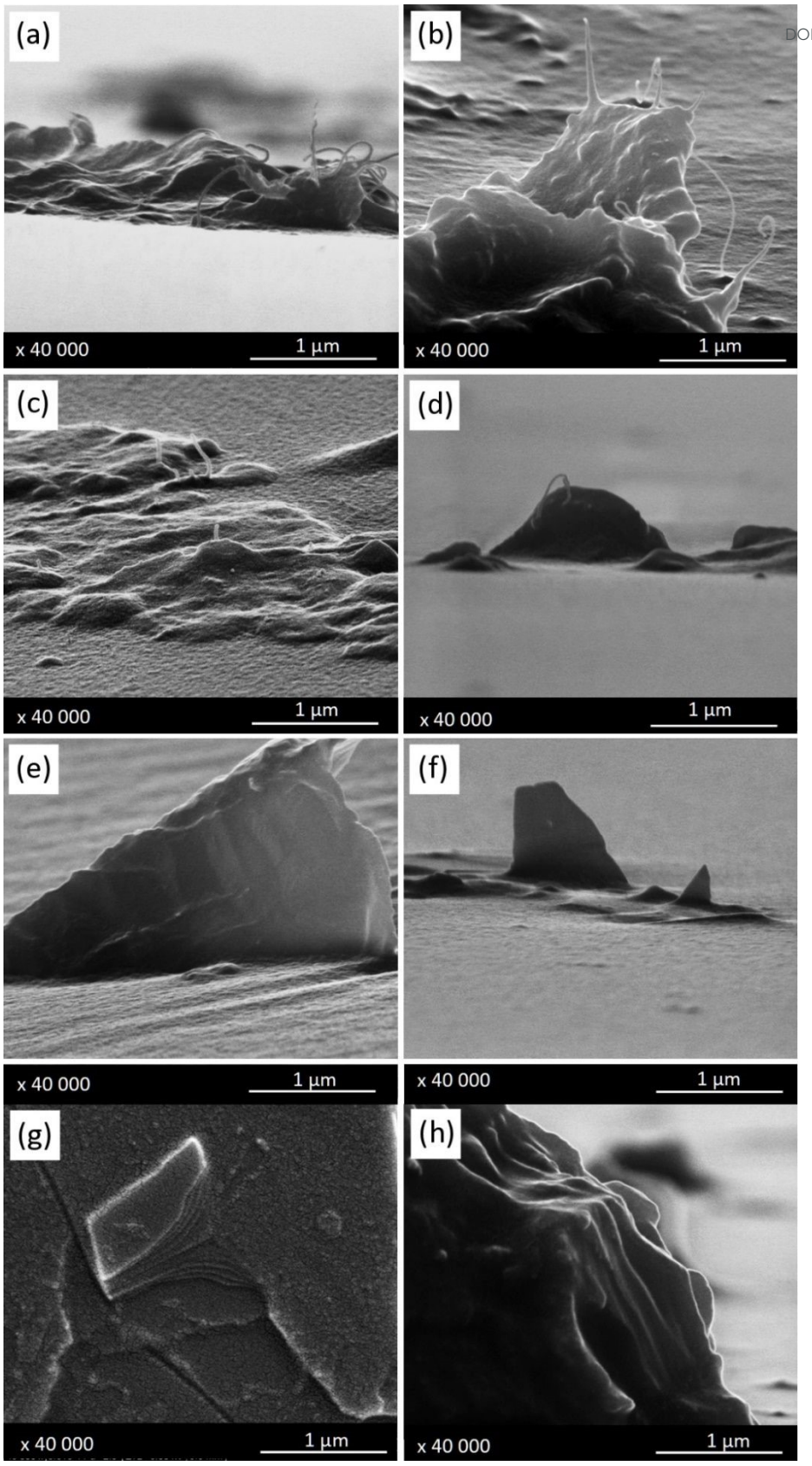

Figure 4: SEM observation of CNM on silicone materials: (a, b) DWCNT; (c, d) DWCNT Ox ; (e, f) FLG ; (g, h) GO on silicone : left column (a, c, e, g) silicone S184 ; right column (b, d, f, h) silicone MED.

View Article Online
DOI: 10.1039/D4NR02810D

Carbon nanotube agglomerates were observed on the surface of both silicones (raw DWCNT: Figure 4 (a, b), DWCNT Ox: **Error! Reference source not found.** (c, d)). Bundles of carbon nanotubes present within these agglomerates are visible. These observations correspond to the ones of the DWCNT agglomerates on Figure 1 (b) or DWCNT Ox on Figure 2 (b), where clusters and bundles of nanotubes were already evidenced. CNM seem to emerge from the silicone while being partly embedded. Similarly, FLG (Figure 4 (e, f)) and GO (**Error! Reference source not found.** (g, h)) nanoparticle clusters are also observed at the surface of both silicones. Graphitic layers may be discerned on all these samples and also seem to emerge from the silicone. SEM observations having been performed after the 2-minute bath sonication cleaning step, it is therefore assumed that they are properly anchored at the surface of both silicone materials.

To confirm this hypothesis, AFM measurements were carried out and an example is shown for GO deposited on both silicones (**Error! Reference source not found.**), while AFM data for other CNM are in supplementary data (Fig. S9-S12). Force curves were recorded according to a matrix of 256x256 positions on an area of 10x10 μm^2. Multiple parameters may be extracted from each force curve [34], including the surface topology, adhesion, and force curve slope that provide information on the rigidity of the sample. Topology, adhesion and rigidity maps can thereafter be reconstituted from these measurements, where the intensity of the parameters is represented on a colour scale (**Error! Reference source not found.**). To complete these maps, these values (65 536 per map) were grouped into histograms to study their distribution on the different analysed materials. AFM measurements performed on SYLGARD184 (S184), a silicone reference sample reveal a uniform smooth surface. The absence of colour changes on the different maps produced (**Error! Reference source not found.** (a-c)), evidences that there is no variation in height, adhesion and slope on the

View Article Online
DOI: 10.1039/D4NR02810D

analysed surface. This information is confirmed by the height profile and the histograms produced from the recorded force curves (**Error! Reference source not found.Error! Reference source not found.** (d-f)). The height profile of a cross-section of the sample surface (Figure 5 (d)) indicates a very smooth surface with a rather small variation in height, less than 5 nm. The histograms show that all the values are grouped, which means that there is no variation in the data. Data obtained for MED silicone (without any deposit), CMC control on S184 (after washing), and CMC control on MED (after washing) materials are not shown but were equivalent to S184. No variation in height, adhesion and slope was observed on these samples surfaces which were all smooth and uniform.

Maps obtained for the GO deposit on silicone samples confirm the presence of clusters of nanoparticles on the surface of both materials (Figure 5 (g, m). Height maps along with height cross-section data indicate that the GO nanoparticles are situated above the silicone surface. Different situations are observed regarding adhesion and slope measured values for the GO clusters present on both silicones. GO nanoparticles on S184 maps present a wide range of adhesion (Figure 5 (h, k)) and slope (Figure 5 (i, l)) values, much larger than observed on the control S184 material (Figure 5 (e, f)). The situation illustrated in the case of GO/MED is rather different, with a much narrower range of adhesion distribution and a bimodal distribution of the slope. While we have shown typical examples of each deposit of the two different silicones, rather different situations were observed, but all indicating that GO agglomerates are definitely anchored in both silicones. The widening of the distribution of both the adhesion force and slope also illustrates that many more different cases may be encountered where the particles may be covered with a variable thickness of silicone, or even no silicone at all, or may finally be located more or less deep in the silicone. Similar observations were made on the other samples (deposits of DWCNT, DWCNT Ox and FLG).

View Article Online
DOI: 10.1039/D4NR02810D

Figure 5 only shows a selection of representative images (Fig. S9-S12 are provided as other examples).

View Article Online
DOI: 10.1039/D4NR02810D

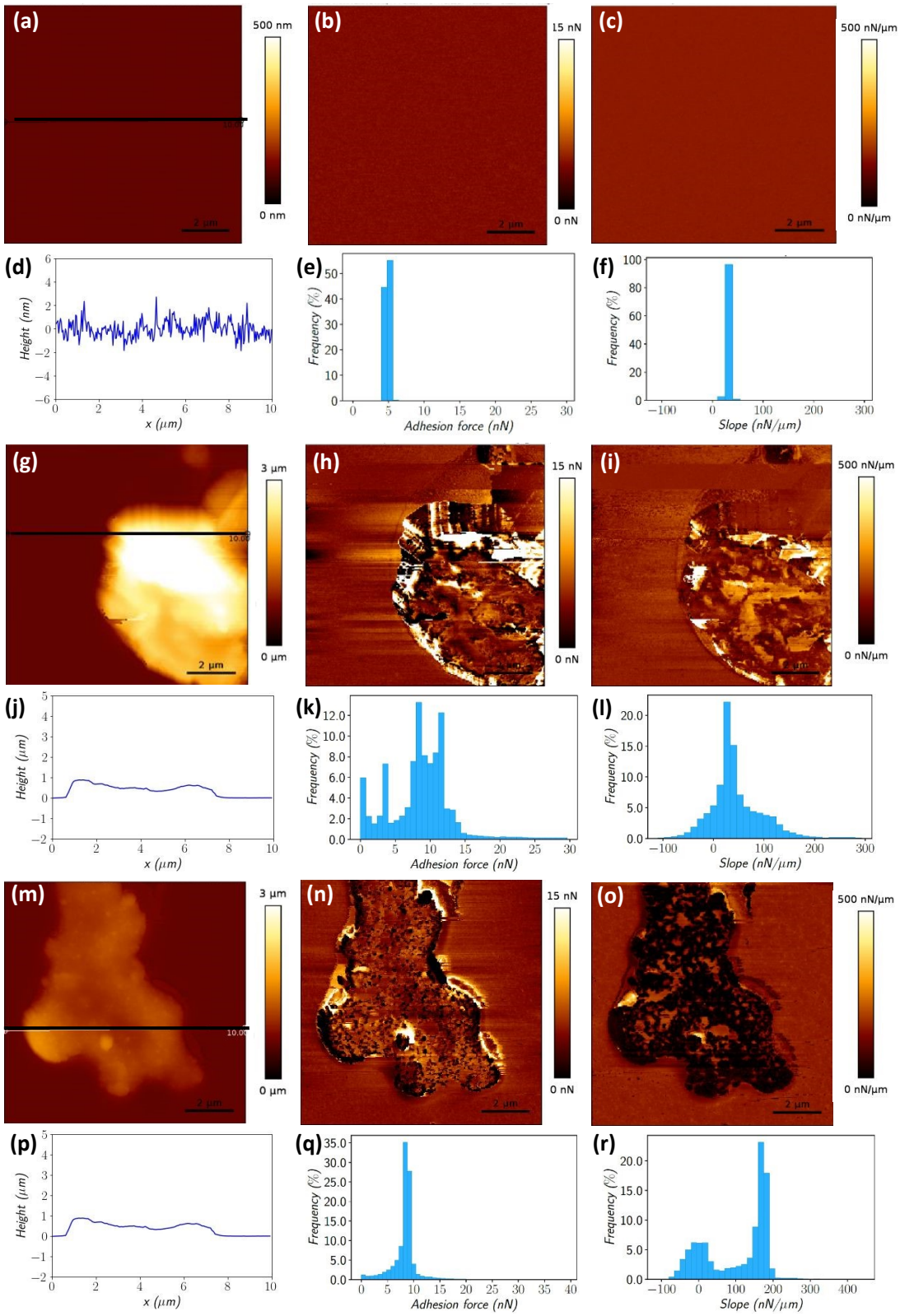

Figure 5: AFM multiparametric imaging (topography, adhesion and rigidity) of silicone S184 reference (a-f), GO / S184 (g-l) and GO / MED (m-r): (a, g, m) height maps; (b, h, n) adhesion maps; (c, i, o) slope maps; (d, j, p) height cross-sections; (e, k, q) adhesion distribution histograms; (f, l, r) slope distribution histograms.

View Article Online
DOI: 10.1039/D4NR02810D

Spatially-resolved 3D (confocal) Raman micro spectroscopy mappings were carried out on the GO / S184 samples, (**Error! Reference source not found.**6 (b)) and GO / MED (**Error! Reference source not found.**6 (d)). The analysed surface as well as the Z amplitude of the samples was selected to present clusters of nanoparticles of several sizes to study different configurations (**Error! Reference source not found.**6). For all the spectra, the Raman signals (point analyses or maps) characteristic of the G band (sp^2) of the GO at 1530 cm^{-1} and the C-H bands of the silicone at between 2800 cm^{-1} and 3100 cm^{-1} have been respectively integrated into each point. The red and green colours were chosen to identify the integration of the GO band and the silicone to create the 3D distribution maps of two deposits of GO on S184 and GO on MED. The spatially resolved maps in 3 dimensions show particles randomly distributed above the surface as well as inside the matrix. There are different configurations with nanoparticle clusters of different sizes that seem to be more or less submerged in the polymer and emerging from the surface, whatever the silicone used.

Raman analyses were carried out on a localised point situated on a GO cluster on the surface of the samples (**Error! Reference source not found.**6 (e, g)). To obtain information about the anchoring of the nanoparticles in the silicone and also if they are emerging from it, several spectra were acquired on this point along the z-axis over an amplitude ranging from +3 µm to -10 µm with respect to the zero plane (**Error! Reference source not found.**6 (f, h)). These analyses were carried out on both GO / silicone samples. The depth profiles clearly show in both cases that the GO agglomerates not only emerge from the surface but are also embedded in the silicone. It seems that the ratio between the relative intensities of GO and silicone signatures gradually reverses as depth in the polymer increases.

View Article Online
DOI: 10.1039/D4NR02810D

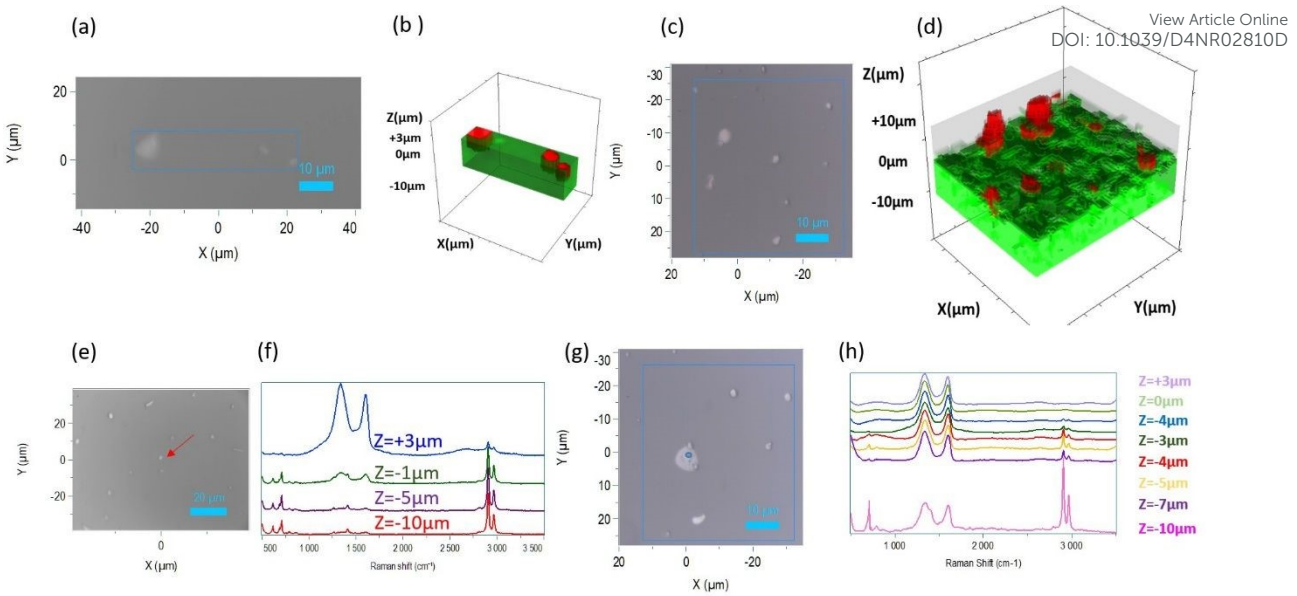

Figure 6: Raman analyses of GO on silicone; (a, c) 2D optical images with a boxed location and (b, d) corresponding 3D Raman maps with silicone depicted in green and the emerging GO represented in red, (e, g) 2D optical images with a boxed location and (f, h) corresponding confocal analysis; (a, b, e, f) GO / S184 and (c, d, g, h) GO / MED.

Spatially-resolved 3D (confocal) Raman micro spectroscopy mappings were also carried out on the DWCNT Ox / S184 (**Error! Reference source not found.**7 (a, b)), and DWCNT Ox / MED (**Error! Reference source not found.**7 (c, d)) samples. As before the analysed surface as well as the Z amplitude of the samples was selected to present clusters of nanoparticles of several sizes to study different configurations. For all spectra, the G' band at 2650 cm^{-1} and the C-H stretching band at 2960 cm^{-1}, which are Raman characteristics signal of the DWCNT Ox and the silicone respectively, were integrated (we chose to integrate bands of equivalent sensitivity). The maps show clusters of nanoparticles randomly distributed on the surface as well as inside the polymer. These clusters seem more or less immersed in the silicone and the two maps represent clusters emerging from the silicone surface.

View Article Online
DOI: 10.1039/D4NR02810D

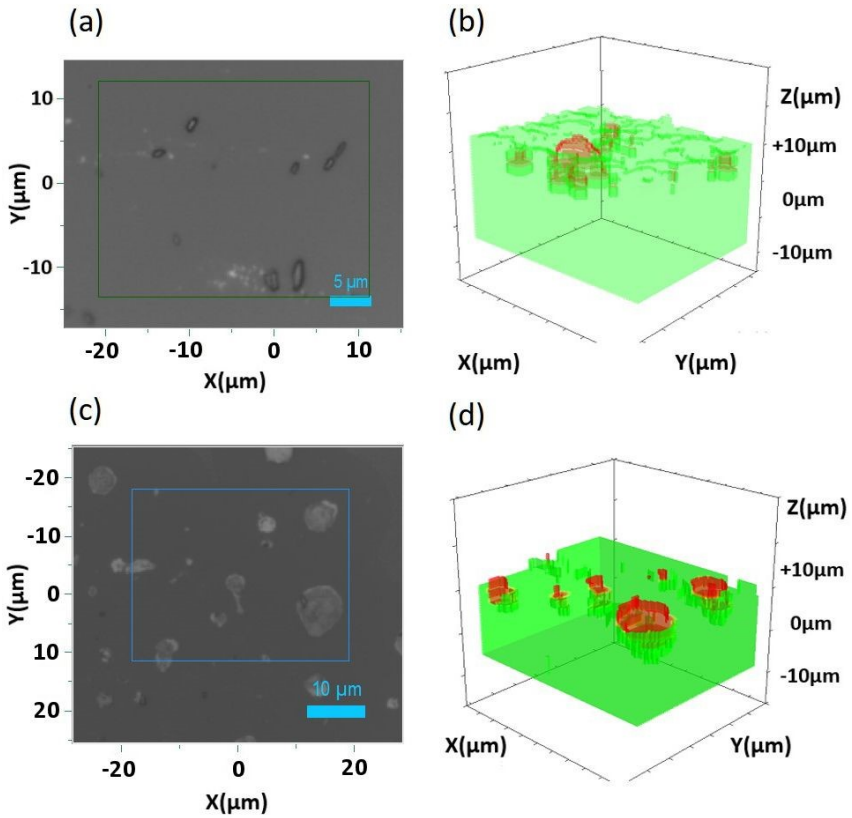

Figure 7: Raman analyses of DWCNT Ox on silicone (a, c) 2D optical image with a boxed location and (b, d) corresponding 3D Raman map with silicone depicted in green and the emerging DWCNT Ox represented in red ; (a, b) DWCNT Ox / S184 and (c, d) DWCNT Ox / MED.

The comparison of data obtained from three different characterization methods carried out on the samples allows us to conclude that airbrush deposition of water-based CNM inks is an effective way to anchor these nanomaterials at the surface of silicone. The different characterization methods complement each other and evidence clusters of nanoparticles (where bundles and platelets may be distinguished) that are both anchored and emerging from the matrix. It differs from most studies in the literature where CNM are fully embedded in the support (nanocomposites), or simply deposited with no evidence of efficient anchoring. The fact that only large agglomerates are visible at the surface of silicone does not exclude the presence of smaller particles in between, which are more difficult to evidence due to the

View Article Online
DOI: 10.1039/D4NR02810D

resolution or sensitivity depending on the characterisation tool. This means that the amount of CNM at the surface may be much larger than what is evidenced here.

3.3 Investigation of the antimicrobial activity

3.3.1 Antibacterial activity of CNM:

Figure 8 summarizes the experimental protocols which were used in this work (see sections 2.4 to 2.7).

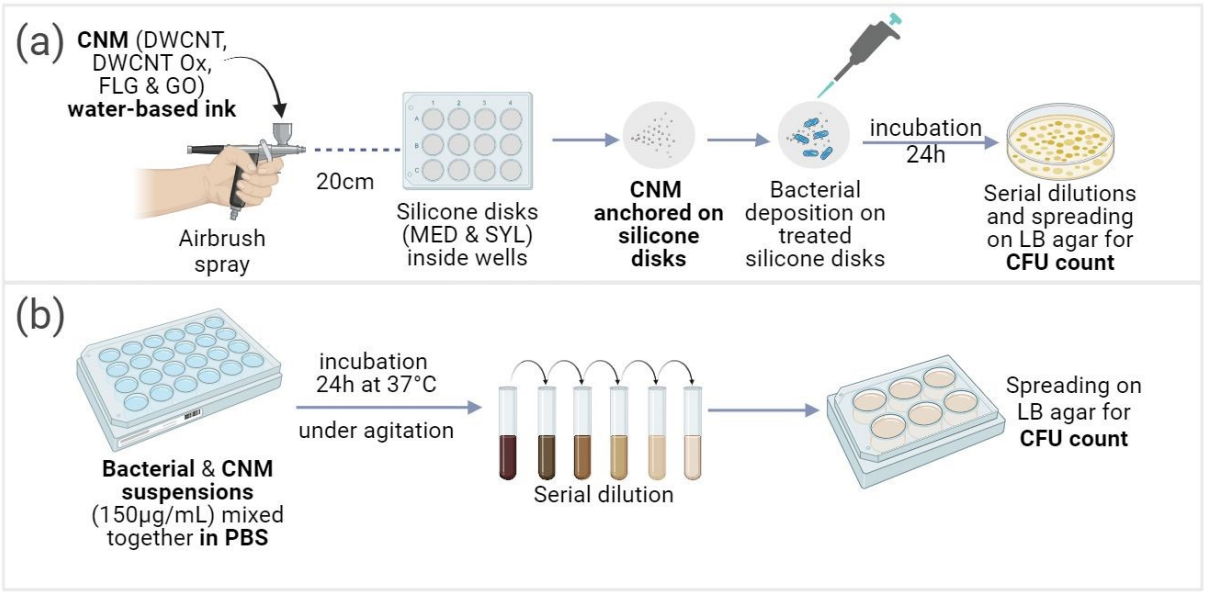

Figure 8: Visual representation of the protocols employed to test for antibacterial activity of CNMs (a) after anchoring on the surface of silicone disks and (b) in suspension.

CFU tests were performed on CNM/silicone deposits (Figure 8 (a)) against *P. aeruginosa* and *S. aureus* bacteria (Figure 9). None of the silicones exhibited any intrinsic antibacterial activity, indicating that even if their composition was certainly different (exact composition of commercial silicones in not possible to obtain), the possible presence of hardener residues did not have any impact. The tested suspensions of CNM in PBS (Figure 8 (b)) did not exhibit any antibacterial activity neither on *P. aeruginosa* bacteria nor on *S. aureus* bacteria (Figure 9 (a-d)). Only oxidised CNM exhibited some antimicrobial activity as deposits on silicones (Figure 9 (e-l)). Among the different tested materials, deposits of GO on silicone samples exhibited very

View Article Online
DOI: 10.1039/D4NR02810D

strong antibacterial activity against *P. aeruginosa* (Figure 9 (i, j)) but not against *S. aureus* (Figure 9 (k, l)). On the contrary, deposits of DWCNT Ox exhibited a very strong antibacterial activity against *S. aureus*, but not against *P. aeruginosa*. Since no antibacterial activity could be evidenced for in the presence of non-oxidized CNM, we cannot exclude the presence of traces of adsorbed CMC which may inhibit their possible antibacterial activity. However, as the washing steps were proved to be rather efficient, it is supposed that only limited amounts of CMC may still be adsorbed. CMC contains carboxylic functions, which are also present at the surface of oxidised CNM.

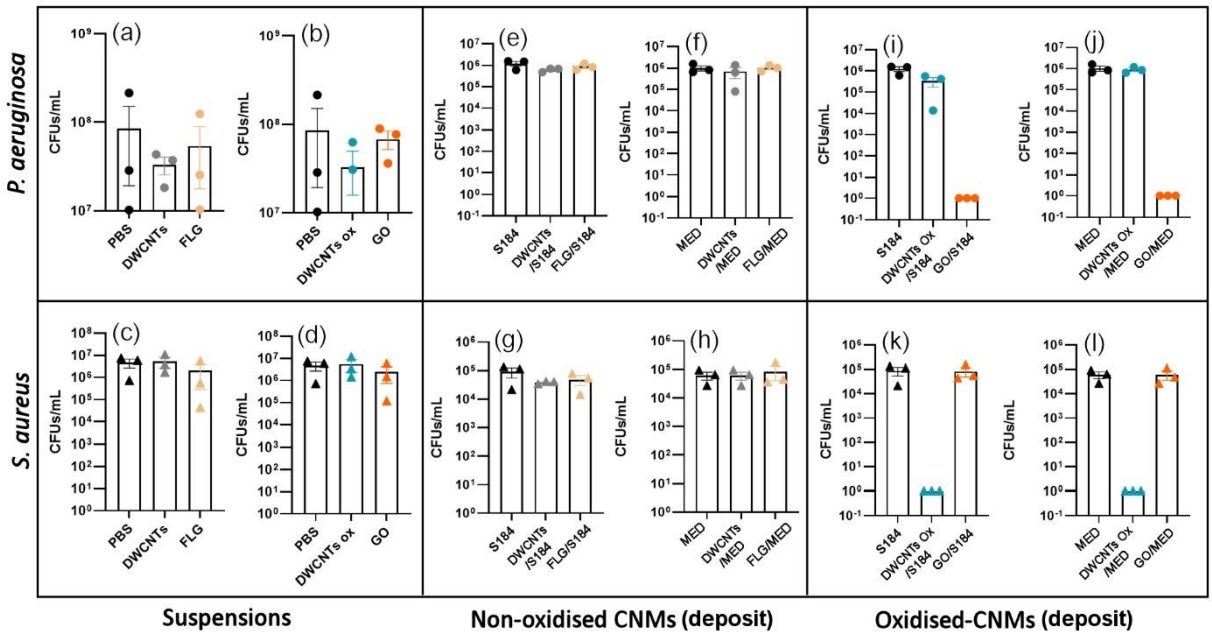

Figure 9: (a-d) ***Antibacterial effect of suspensions of CNM*** *(150 µg.mL-1) on P. aeruginosa of: (a) non-oxidised CNM suspension, (b) oxidized CNM suspension, and on S. aureus of: (c) non-oxidised CNM suspension and (d) oxidized CNM suspension. (e-h)* ***Antibacterial effect of deposits of non-oxidized CNM*** *on* P. aeruginosa*: (e) on S184, (f) on MED, and on* S. aureus*: (g) on S184, (h) on MED.* ***(i-l) Antibacterial effect of deposits of oxidized CNM*** *on* P. aeruginosa*: (i) on S184, (j) on MED, and on* S. aureus*: (k) on S184, (l) on MED. Data is illustrated as the mean of at least n = 3 independent experiments represented by circles for P. aeruginosa and triangles for S. aureus, with error bars indicating SD. The colour code corresponds to the different kinds of CNM.*

3.3.2 Antiviral properties of CNM:

View Article Online
DOI: 10.1039/D4NR02810D

Here to quantify viral load, we assess the ability of the virus to kill infected cells (TCID50 assay) as previously described [31]. As in the previous investigation of the antibacterial load, it is mandatory to first check whether any CNM particle that may detach or not from the surface of the support material may exhibit a direct toxicity towards Vero E6 cells used for viral load quantification. We thus first evaluated the cytotoxicity of CNM on Vero E6 cells. Cells were incubated with different doses of CNM (from 1.25 to 150 µg.mL^{-1}) for 3 days and toxicity was evaluated by LDH release assay. The highest concentration of 150 µg.mL^{-1} would correspond to the release of all the CNM deposited on the material placed at the bottom of a given culture well. As shown in Figure 10 (a), none of the CNM exhibited any toxicity towards Vero E6 cells, whatever the tested dose, which allows us to exclude any possible false positive antiviral activity. To determine the viral load to be used in our experiments, we evaluated the kinetics of SARS-CoV-2 infectivity with time. Three different doses of SARS-CoV-2 (10^3 to 10^7 PFU) were incubated for 6 to 48 h at 37°C. Viral load was measured by TCID50 assay. As shown in Figure 10 (b), we observed the expected decrease in virus load over time.

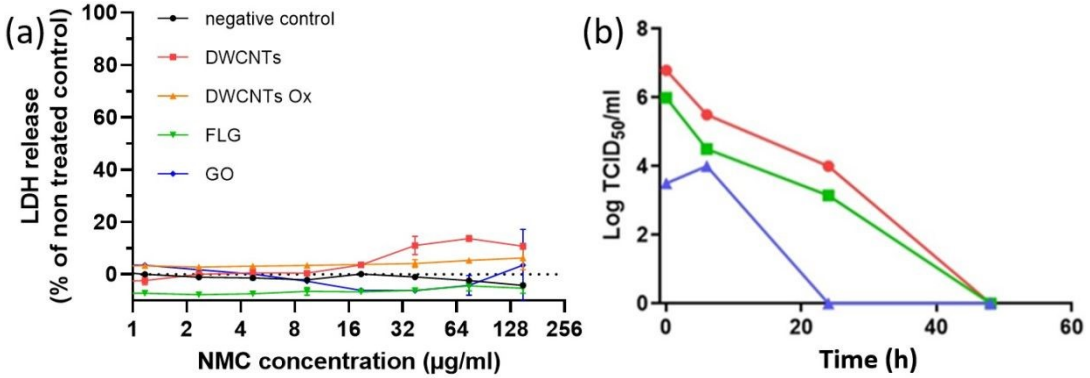

Figure 10: (a) Cytotoxicity of CNM on Vero E6 cells measured by LDH release assay after 3 days of incubation; Data are expressed as mean +- SD of 2 independent experiments. (b) kinetics of SARS-CoV-2 load decrease vs time in DMEM cell culture medium (red: : 10^3 PFU; green: 10^6 PFU; blue: 10^7 PFU).

View Article Online
DOI: 10.1039/D4NR02810D

From the obtained result, we decided to test the viricidal activity of CNM with the intermediate dose of 10^6 PFU at 24h. CMC control corresponds to a spray of CMC at 1 $mg.mL^{-1}$ used as a control in case of incomplete washing. As shown in Figure 11, none of the CNM presented any significant viricidal effect against SARS-CoV-2 on any of the tested substrates. The conclusion is the same for the commercial graphene mask that we have tested as a comparison (Figures S6-S8)

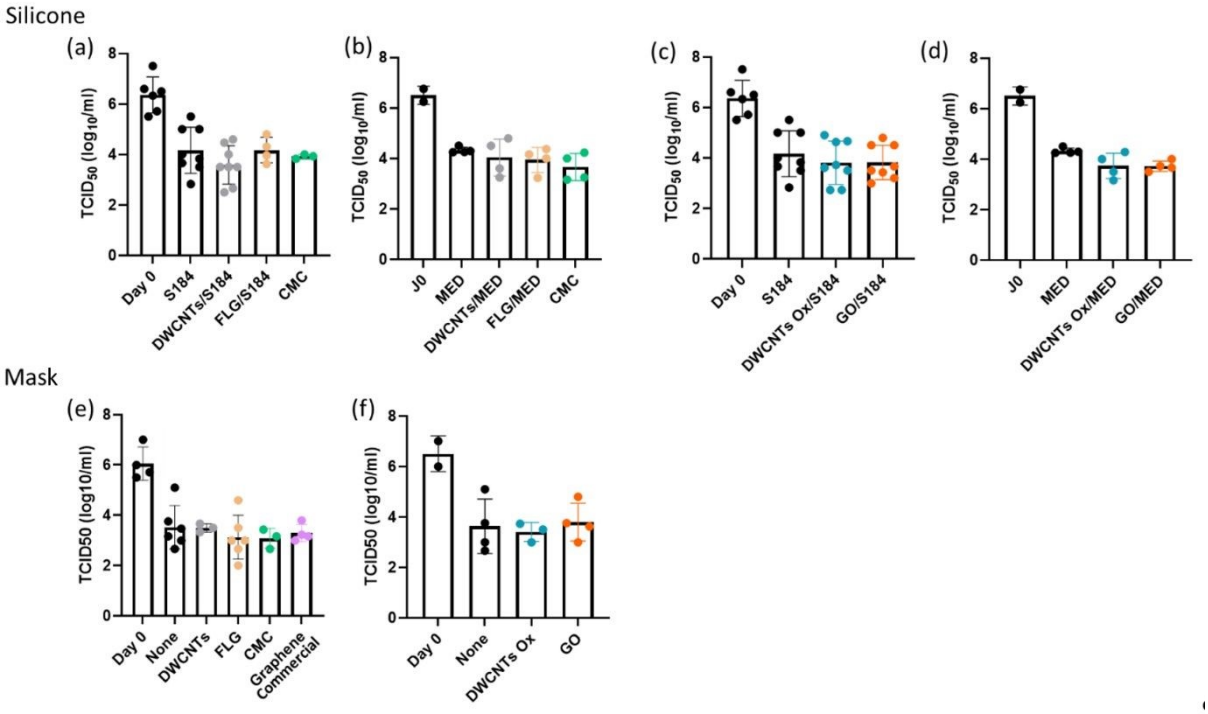

Figure 11: antiviral effect on SARS-CoV-2 of (a) non-oxidised CNM deposited on S184, (b) oxidized CNM deposited on S184, (c) non-oxidised CNM deposited on MED, (d) oxidized CNM deposited on MED, (e) non-oxidised CNM deposited on classical (FFP1) surgical mask, (f) oxidized CNM deposited on classical (FFP1) surgical mask. In (e) is included the result of the test of the commercial graphene mask (Graphene Commercial). Data is illustrated as the mean of at least n = 2 independent experiments represented by circles, with error bars indicating SD. The colour code corresponds to the different kinds of CNM.

3.4 Discussion

The different characterization methods performed on the materials after 2 min of ultrasound cleaning complement each other. At both low and high magnification, SEM

View Article Online
DOI: 10.1039/D4NR02810D

observations showed clusters and bundles or platelets of CNM homogeneously dispersed on the material surface. AFM analysis revealed all possible configurations with small clusters with an elevation of *ca.* 100 nm from the silicone surface, whereas some bigger clusters presented an elevation of around 1 µm from the silicone surface. Raman analyses proved that CNM clusters were both blocked and emerging from the surface. Several elaboration methods are reported in the literature for the development of antimicrobial composites based on CNM, such as electrospinning [13–15], 3D printing [16–18], dip coating [19,20], *etc.* However, these nanocomposites contain the nanoparticles within the whole matrix. Very few methods allowing CNM to emerge from a polymer matrix are described in the literature and are usually based on the removal of the matrix at the top surface of a nanocomposite. As an example, A UV/O_3 oxidation treatment on GO nanosheets allowed etching away the surface polymer (2-hydroxyethyl methacrylate (HEMA)) and direct access to the nanoparticles was reported [21]. Another mentioned method is laser ablation which was able to resurface GO nanoparticles embedded in an agarose matrix by liquefaction and matter transport [22]. Hence, we have demonstrated in the case of silicone that CNM may be transferred effectively at the surface using airbrush deposition, and we have also shown that the dispersant required in the case of non-oxidised CNM to prepare a stable suspension could be removed by a 2-min bath-sonication cleaning in water, while keeping the CNM anchored at the surface of the coated material.

Our results show that after deposition on silicone, only GO had a strong impact, and only on *P. aeruginosa*, while only oxidised DWCNT had a strong impact on *S. aureus*. The majority of studies suggest the antimicrobial mechanisms of the CNM after employing techniques such as SEM (to identify morphology changes) and staining followed by fluorescence microscopy [51-53]. These mechanisms cannot be universally applied, as this

View Article Online
DOI: 10.1039/D4NR02810D

greatly depends on the physical characteristics of the CNM employed (such as structure, specific surface area, length, diameter, and the presence of functional groups on the surface) [51,54]. However, it is globally assumed that CNM exert their antimicrobial activity based on three modes of action: through mechanical stretching or piercing, physical interaction with the cell membrane resulting in wrapping and isolation from its nutritive surrounding, and/or through the generation of Reactive Oxygen Species (ROS) resulting in oxidative stress, thus disrupting the bacterial cell membrane (due to lipid peroxidation) [51,55-56]. It is worth noting that only oxidised materials exhibited antibacterial activity after deposition on silicone, while none of them had any activity on the same bacteria while in suspension. This suggests that the presence of the oxygen-containing groups present at the surface plays a major role.

In the case of the deposited CNM, the washing step proved to be effective for the removal of surface CMC also deposited together with CNM (Fig. S3), although the total removal of CMC is both difficult to assess and relatively unlikely. These observations suggest that not only the shape of the CNM is important, but also their surface chemistry. The surface of oxidised CNM being much more chemically reactive, may induce higher levels of oxidative stress within bacteria after interaction with the membranes. Gram-negative bacteria have a thin peptidoglycan layer of 6 to 15 nm and an additional outer lipid membrane whereas Gram-positive bacteria have a thick peptidoglycan layer of (20-80 nm) and miss the outer lipid membrane. Thus, the test results may be related to the differences between the cell walls of Gram-positive and Gram-negative bacteria and the different morphologies between the tested CNM. For example, it has been reported that Gram-positive bacteria such as *S. aureus* may be more susceptible to the piercing effect of needle shaped CNTs [57], while gram-negative *P. aeruginosa* is assumed to be more susceptible to the 'nano knife' and wrapping effect of GO. In addition, the shape of the bacteria may also impact the selectivity of CNM,

View Article Online
DOI: 10.1039/D4NR02810D

and CNT may have more effect against spherical-shaped *S. aureus* bacteria than on rod-shaped *P. aeruginosa* bacteria [48]. However, it is difficult to conclude on the active mechanisms in this study through literature analysis as the available literature can be contradicting. For example, Rogala-Wieglus argue in their state of art that on the contrary, Gram-negative bacteria such as *P. aeruginosa* and *E. coli* are more susceptible to the piercing effect of CNTs [56]. In addition, Diez suggests that membrane harm induced by GO is more damaging towards Gram-positive bacteria than Gram-negative bacteria [55]. Hence the importance of exploring the mechanisms exerted by the CNM employed in this study further, by techniques mentioned below.

Our results show that the initial assumption that CNM active in suspension would also be active after deposition on a surface was obviously not correct. The difference between these two configurations may come from their mobility. CNM incubated with bacteria in suspension can move freely within the volume, potentially resulting in less direct contact between the two. Whereas CNM fixed on silicone surface resulted in enhanced contact with the microorganisms, as the bacterial suspension was directly deposited on the treated surface. We also show that GO and oxidised DWCNT exhibited the same antibacterial activity on both silicones, suggesting that the airbrush coating method may be used on several different supports to elaborate CNM-based antimicrobial surfaces. This hypothesis will be investigated in further works. As mentioned previously, although the exact antibacterial mechanisms were not investigated in this preliminary work, AFM will be used to investigate the mechanical impact of the tested materials on microorganisms [29,49,50]. Damages to cell membranes by the generation of reactive oxygen species (ROS) will also be investigated using markers of lipid peroxidation [20]. In addition, the proportion of live and dead bacteria will be evaluated by fluorescence measurements (live-dead assay) and compared to SEM images to assess the

View Article Online
DOI: 10.1039/D4NR02810D

distribution of CNM at the surface and the morphology of the exposed bacteria. The size of the investigated bacteria in this work is typically between 0.5 and 5 µm, *S. aureus* being slightly smaller than *P. aeruginosa*. The images of the surface of silicone after spray deposition all show rather larger agglomerates, which are separated by distances that look larger than the size of the bacteria. However, as already discussed, it is likely that smaller agglomerates, or even individual particles, may also be present in between. The contact-killing hypothesis should thus still be valid.

Finally, in the context of COVID-19 pandemic, graphene and related materials have attracted attention with the commercialization of graphene-based respiratory masks, claimed to exhibit some viricidal activity. Previous work has already been performed and reported antiviral activity against SARS-CoV-2 from masks spray-coated with carbon nanotubes and masks with a carbon nanotube filter [25,26]. However, although the principle of coating a surface with a CNM by spray-deposition was indeed the same, it must be noted that the role of the used CNM (carbon nanotubes) was mainly to bring superhydrophobicity in the work of Soni et al. [25], which is not the case in this work, for none of the investigated CNM. They also used a benzene-based ink, while we developed a water-based approach. In the work of Lee et al. [26], the CNT were directly integrated in dry form using a very specific approach which cannot be generalised to other commercial sources of carbon nanotubes. Our results with two different morphologies (1D, 2D) and two different surface chemistries (oxidised CNM or not) have not revealed such effect against SARS-COV2, whatever the tested support on which they were deposited (silicone, or respiratory mask). In this preliminary work, we have not checked the possible release of CNM in the medium, possibly leading to false results. However, we checked that the incubation of Vero E6 cells at concentrations higher than what could be achieved in case of the total release of deposited CNM had no impact on these cells.

View Article Online
DOI: 10.1039/D4NR02810D

This allows us to rule out any possible interference. As in the case of the investigation of the antibacterial activity, this work will require more in-depth investigations (in progress). However, the absence of viricidal activity in the commercial mask is still valid and raises questions.

Although the antimicrobial impact of CNM has been largely described in the literature, most works were dealing with direct contact with particles in suspension in the exposure medium [20,35–38]. This work focused on investigating the antimicrobial activity of the elaborated materials against Gram- type *P. aeruginosa* and Gram+ type *S. aureus* bacteria by measuring the capacity of bacteria to form colonies after incubation with the materials. No antimicrobial activity from the different CNM suspensions was evidenced from our work. These results are in contradiction with some earlier publications dealing with similar CNM. However, the large variability in terms of results may also easily be explained by the differences in terms of the CNM themselves, the tested concentrations and experimental conditions (duration, medium composition, *etc*.). This is the main reason why we decided in this work to investigate simultaneously two monodimensional (1D) and two bidimensional (2D) morphologies, including the as-produced and an oxidised form, to also include this very important aspect. Indeed, the oxidation of CMNs typically increases significantly the stability of suspensions in aqueous medium, which leads to increased impact due to better interaction with cells. In our work, we have added CMC, a food additive (E466), to suspensions of non-oxidised CNM (DWCNT and FLG) to overcome the stability issue, after checking that the dispersant itself did not have any impact. This issue was recently discussed in the framework of OECD test guidelines for the environmental impact of graphene and related materials, where the addition of a dispersant is accepted [39]. This appears in contradiction with our earlier work on the same non-oxidised DWCNT in which a moderated activity towards *P.*

View Article Online
DOI: 10.1039/D4NR02810D

aeruginosa was demonstrated using the same assay, at similar concentrations of both CNM (100 µg.mL^{-1}, while we used 150 µg.mL^{-1} in this work) and bacteria, for the same exposure duration of 24 h. Furthermore, in this same work, we described a very strong activity against *S. aureus*, that we have not reproduced here. The only difference between these 2 works is the presence of CMC in this work (which does not exhibit any intrinsic antibacterial activity), which would suggest that a better dispersion does not help to fight against *P. aeruginosa* and *S. aureus*. However, the antibacterial activity of both GO and rGO in suspension was reported by Gurunathan *et al.* against *P. aeruginosa* via oxidative stress induction [40], while the exact bacterial concentration is unknown. CNT ability to inhibit the proliferation of *S. aureus* was also reported [35,41]. These contradictory results may be explained not only by the differences between the CMNs themselves, but also between all the other experimental parameters, including the way the CFU assay was performed [41–43].

In this work, our initial work hypothesis was that if some antimicrobial activity was observed with CNM in suspension, it should be transferred to the surface of a material after coating with the same suspension – based on the commonly accepted assumption that the main antimicrobial mechanisms associated to CNM involve direct contact with the microorganisms. This direct contact is not possible when CNM are included within a matrix making up a nanocomposite. A few methods have been proposed in the literature to prepare antimicrobial composites based on carbon nanomaterials but they mostly described fully embedded nanoparticles into the polymeric matrix [44–47]. Rare approaches allowing a direct access to CNM embedded in polymer may be found, such as the use of a UV/O_3 oxidation treatment to etch away the surface polymer, or the use of laser ablation that allows embedded nanoparticles to resurface from the matrix [21,22]. This work has thus focused on blocking the carbon nanoparticles on a polymeric surface while also allowing them to emerge

View Article Online
DOI: 10.1039/D4NR02810D

from this surface to enable direct contact between microorganisms and CNM while ensuring the durability of action without loss of nanoparticles and no toxicity issue related to released nanoparticles.

4. CONCLUSION

We have shown that airbrush coating is a suitable method to elaborate CNM-based antimicrobial surfaces on silicone, comparing the two most investigated carbon nanomaterials, carbon nanotubes and few-layer graphene. Because surface chemistry usually plays a major role, we also included their oxidised counterparts. Characterisation of the deposits combining SEM, AFM and Raman spectroscopy 3D mapping demonstrate that airbrush coating allowed to anchor all the tested CNT at the surface of two different silicone materials, used in very different fields of applications (microfluidics and coating of electronics for Sylgard 184, and the biomedical field for MED-4729). The investigation of antimicrobial activity of CNM-coated surfaces was also investigated: antibacterial activity against Gram-negative (*P. aeruginosa*) and Gram-positive (*S. aureus*) bacteria, viricidal activity against SARS-COV2. While none of the tested CNM exhibited any antibacterial activity in suspension, GO and oxidised DWCNT deposited on silicone exhibited strong antibacterial activity against *P. aeruginosa* and *S. aureus*, respectively. This highlights the impact of the complex interplay between shape, surface chemistry, and mobility of the CNM on their antibacterial activity. Most available studies of the antimicrobial properties of CNM-containing composites do not detail the exact antimicrobial mechanisms but mainly assume that typical effects of particles free in a liquid medium (essentially oxidative stress) may be transferred to a surface, without checking this hypothesis. We have demonstrated here that this assumption is not always true.

View Article Online
DOI: 10.1039/D4NR02810D

As carbon nanomaterials are effectively blocked on the silicone surface and are chemically resistant, we expect no loss of activity with time, while the long-term impact of biofilms will also need to be investigated in further work. The absence of a viricidal effect against SARS-COV2 suggests that considering the possible negative impact of such nanomaterials after inhalation, it may be safer not to include them in respiratory masks in the absence of clear evidence of a real sanitary benefit. This also highlights the need to ban the use of "graphene" as a generic description of 2D carbon-based nanomaterials because very different nanoparticles may be included, such as GO and FLG, exhibiting very different safety concerns.

CONFLICTS OF INTEREST

The authors declare no conflict of interest.

DATA AVAILABILITY

Some of the data supporting this article have been included as part of the Supplementary Information. All data can be made available upon request to the corresponding author (Emmanuel.flahaut@univ-tlse3.fr).

ACKNOWLEDGEMENTS

This research was funded, in whole or in part, by University Paul Sabatier Toulouse 3 (France), Grant TREMPLIN 2021, CARBO-COVID. The authors warmly acknowledge the ANEXPLO Animal Facility Level 3 of the IPBS institute for technical assistance with SARS-CoV-2 handling. We thank A. Renard from the spectroscopy and microscopy Service Facility (SMI) of LCPME (UMR 7564).

View Article Online
DOI: 10.1039/D4NR02810D

REFERENCES

[1] Cámara, M, Green, W, MacPhee, CE, et al. Economic significance of biofilms: a multidisciplinary and cross-sectoral challenge, Npj Biofilms Microbiomes, 8 (2022) 42.

[2] Ciofu, O, Moser, C, Jensen, PØ, et al. Tolerance and resistance of microbial biofilms, Nature Reviews Microbiology, 20 (2022) 621-35.

[3] Brown, DC, Okpala, GN, Gieg, LM, et al. Chapter 12 - Biofilms and their role in corrosion in marine environments. Understanding Microbial Biofilms, 2023, p. 173-85.

[4] Zander, ZK, Becker, ML. Antimicrobial and Antifouling Strategies for Polymeric Medical Devices, ACS Macro Lett., 7 (2018) 16-25.

[5] Vaidya, MY, McBain, AJ, Butler, JA, et al. Antimicrobial Efficacy and Synergy of Metal Ions against Enterococcus faecium, Klebsiella pneumoniae and Acinetobacter baumannii in Planktonic and Biofilm Phenotypes, Sci Rep, 7 (2017) 5911 : 1-9.

[6] Pant, B, Pokharel, P, Tiwari, AP, et al. Characterization and antibacterial properties of aminophenol grafted and Ag NPs decorated graphene nanocomposites, Ceramics International, 41 (2015) 5656-62.

[7] Liu, Y, Yang, G, Jin, S, et al. Development of High-Drug-Loading Nanoparticles, ChemPlusChem, 85 (2020) 2143-57.

[8] Dianzani, C, Zara, GP, Maina, G, et al. Drug Delivery Nanoparticles in Skin Cancers, BioMed Research International, 2014 (2014) 1-13.

[9] Riley, PR, Narayan, RJ. Recent advances in carbon nanomaterials for biomedical applications: A review, Current Opinion in Biomedical Engineering, 17 (2021) 100262.

[10] Staneva, AD, Dimitrov, DK, Gospodinova, DN, et al. Antibiofouling Activity of Graphene Materials and Graphene-Based Antimicrobial Coatings, Microorganisms, 9 (2021) 1839 :1-20.

[11] Popov, V. Carbon nanotubes: properties and application, Materials Science and Engineering: R: Reports, 43 (2004) 61-102.

[12] Giraud, L, Tourrette, A, Flahaut, E. Carbon nanomaterials-based polymer-matrix nanocomposites for antimicrobial applications: a review, Carbon, 182 (2021) 463-83.

[13] Liu, Y, Park, M, Shin, HK, et al. Facile preparation and characterization of poly(vinyl alcohol)/chitosan/graphene oxide biocomposite nanofibers, Journal of Industrial and Engineering Chemistry, 20 (2014) 4415-20.

[14] Yang, S, Lei, P, Shan, Y, et al. Preparation and characterization of antibacterial electrospun chitosan/poly (vinyl alcohol)/graphene oxide composite nanofibrous membrane, Applied Surface Science, 435 (2018) 832-40.

[15] Schiffman, JD, Elimelech, M. Antibacterial Activity of Electrospun Polymer Mats with Incorporated Narrow Diameter Single-Walled Carbon Nanotubes, ACS Appl. Mater. Interfaces, 3 (2011) 462-8.

[16] Chen, Q, Mangadlao, JD, Wallat, J, et al. 3D Printing Biocompatible Polyurethane/Poly(lactic acid)/Graphene Oxide Nanocomposites: Anisotropic Properties, ACS Applied Materials & Interfaces, 9 (2017) 4015-23.

[17] Sayyar, S, Cornock, R, Murray, E, et al. Extrusion printed graphene/ polycaprolactone/ composites for tissue engineering, Mater. Sci. Forum, 773 (2013) 496-502.

[18] Sayyar, S, Murray, E, Thompson, BC, et al. Processable conducting graphene/chitosan hydrogels for tissue engineering, J. Mater. Chem. B, 3 (2015) 481-90.

[19] Liu, Y, Wen, J, Gao, Y, et al. Antibacterial graphene oxide coatings on polymer substrate, Applied Surface Science, 436 (2018) 624-30.

View Article Online
DOI: 10.1039/D4NR02810D

[20] Li, R, Mansukhani, ND, Guiney, LM, et al. Identification and Optimization of Carbon Radicals on Hydrated Graphene Oxide for Ubiquitous Antibacterial Coatings, ACS Nano, 10 (2016) 10966-80.

[21] Lu, X, Feng, X, Werber, JR, et al. Enhanced antibacterial activity through the controlled alignment of graphene oxide nanosheets, Proc Natl Acad Sci USA, 114 (2017) E9793-801.

[22] Papi, M, Palmieri, V, Bugli, F, et al. Biomimetic antimicrobial cloak by graphene-oxide agar hydrogel, Sci Rep, 6 (2016) 1-7.

[23] Sengupta, J, Hussain, CM. The Emergence of Carbon Nanomaterials as Effective Nano-Avenues to Fight against COVID-19, Materials, 16 (2023) 1068.

[24] Sengupta, J, Hussain, CM. Carbon nanomaterials to combat virus: A perspective in view of COVID-19, Carbon Trends, 2 (2021) 100019.

[25] Soni, R, Joshi, SR, Karmacharya, M, et al. Superhydrophobic and Self-Sterilizing Surgical Masks Spray-Coated with Carbon Nanotubes, ACS Appl. Nano Mater., 4 (2021) 8491-9.

[26] Lee, S, Nam, J-S, Han, J, et al. Carbon Nanotube Mask Filters and Their Hydrophobic Barrier and Hyperthermic Antiviral Effects on SARS-CoV-2, ACS Appl. Nano Mater., 4 (2021) 8135-44.

[27] Flahaut, E, Bacsa, R, Peigney, A, et al. Gram-scale CCVD synthesis of double-walled carbon nanotubes, Chem. Commun., (2003) 1442-3.

[28] Shahriary, L, Athawale, AA. Graphene Oxide Synthesized by using Modified Hummers Approach, 02 (2014) 6.

[29] Chopinet, L, Formosa, C, Rols, MP, et al. Imaging living cells surface and quantifying its properties at high resolution using AFM in QI^{TM} mode, Micron, 48 (2013) 26-33.

[30] https://www.jpk.com/app-technotes-img/AFM/pdf/jpk-tech-quantitative-imaging.14-1.pdf, (n.d.).

View Article Online
DOI: 10.1039/D4NR02810D

[31] Péricat, D, Leon-Icaza, SA, Sanchez Rico, M, et al. Antiviral and Anti-Inflammatory Activities of Fluoxetine in a SARS-CoV-2 Infection Mouse Model, IJMS, 23 (2022) 13623.

[32] Weibel, A, Mesguich, D, Chevallier, G, et al. Fast and easy preparation of few-layered-graphene/magnesia powders for strong, hard and electrically conducting composites, Carbon, 136 (2018) 270-9.

[33] Flahaut, E, Agnoli, F, Sloan, J, et al. CCVD Synthesis and Characterization of Cobalt-Encapsulated Nanoparticles, Chem. Mater., 14 (2002) 2553-8.

[34] Alsteens, D, Müller, DJ, Dufrêne, YF. Multiparametric Atomic Force Microscopy Imaging of Biomolecular and Cellular Systems, Acc. Chem. Res., 50 (2017) 924-31.

[35] Chen, H, Wang, B, Gao, D, et al. Broad-Spectrum Antibacterial Activity of Carbon Nanotubes to Human Gut Bacteria, Small, 9 (2013) 2735-46.

[36] Azizi-Lalabadi, M. Carbon nanomaterials against pathogens; the antimicrobial activity of carbon nanotubes, graphene/graphene oxide, fullerenes, and their nanocomposites, Adv. Colloid Interface Sci, 284 (2020) 102250 : 1-15.

[37] Liu, S, Zeng, TH, Hofmann, M, et al. Antibacterial Activity of Graphite, Graphite Oxide, Graphene Oxide, and Reduced Graphene Oxide: Membrane and Oxidative Stress, ACS Nano, 5 (2011) 6971-80.

[38] Xin, Q, Shah, H, Nawaz, A, et al. Antibacterial Carbon-Based Nanomaterials, Adv. Mater., 31 (2018) 1804838 : 1-14.

[39] Connolly, M, Moles, G, Carniel, FC, et al. Applicability of OECD TG 201, 202, 203 for the aquatic toxicity testing and assessment of 2D Graphene material nanoforms to meet regulatory needs, NanoImpact, 29 (2023) 100447 : 1-31.

View Article Online
DOI: 10.1039/D4NR02810D

[40] Gurunathan, S, Woong Han, J, Abdal Daye, A, et al. Oxidative stress-mediated antibacterial activity of graphene oxide and reduced graphene oxide in Pseudomonas aeruginosa, IJN, 7 (2012) 5901-14.

[41] Liu, S, Wei, L, Hao, L, et al. Sharper and Faster "Nano Darts" Kill More Bacteria: A Study of Antibacterial Activity of Individually Dispersed Pristine Single-Walled Carbon Nanotube, ACS Nano, 3 (2009) 3891-902.

[42] Arias, LR, Yang, L. Inactivation of Bacterial Pathogens by Carbon Nanotubes in Suspensions, Langmuir, 25 (2009) 3003-12.

[43] Perreault, F, de Faria, AF, Nejati, S, et al. Antimicrobial Properties of Graphene Oxide Nanosheets: Why Size Matters, ACS Nano, 9 (2015) 7226-36.

[44] Sayyar, S. Fabrication of 3D structures from graphene-based biocomposites, J. Mater. Chem. B, 5 (2017) 3462-82.

[45] Lu, B, Li, T, Zhao, H, et al. Graphene-based composite materials beneficial to wound healing, Nanoscale, 4 (2012) 2978-82.

[46] Wang, Y, Zhang, P, Liu, CF, et al. A facile and green method to fabricate graphene-based multifunctional hydrogels for miniature-scale water purification, RSC Adv., 3 (2013) 9240-6.

[47] Mohamed, NA, Abd El-Ghany, NA. Novel aminohydrazide cross-linked chitosan filled with multi-walled carbon nanotubes as antimicrobial agents, International Journal of Biological Macromolecules, 115 (2018) 651-62.

[48] Gomes, M, Gomes, LC, Teixeira-Santos, R, et al. Carbon nanotube-based surfaces: Effect on the inhibition of single- and dual-species biofilms of Escherichia coli and Enterococcus faecalis, Results in Surfaces and Interfaces, 9 (2022) 100090 : 1-9.

[49] Dague, E, Alsteens, D, Latgé, J-P, et al. Chemical Force Microscopy of Single Live Cells, Nano Lett., 7 (2007) 3026-30.

[50] Francois, JM, Formosa, C, Schiavone, M, et al. Use of atomic force microscopy (AFM) to explore cell wall properties and response to stress in the yeast Saccharomyces cerevisiae, Curr Genet, 59 (2013) 187-96.

[51] Moskvitina, E, Kuznetsov, V, Moseenkov, S, et al. Antibacterial effect of carbon nanomaterials: Nanotubes, carbon nanofibers, nanodiamonds, and onion-like carbon. Materials, 16 (2023) 957.

[52] Saleemi, MA, Kong, YL, Yong, PV, et al. An overview of antimicrobial properties of carbon nanotubes-based nanocomposites. Advanced Pharmaceutical Bulletin, 12 (2021) 449-65.

[53] Deokar, AR, Lin, L-Y, Chang, C-C, et al. Single-walled carbon nanotube coated antibacterial paper: Preparation and mechanistic study. Journal of Materials Chemistry B, 1 (2013) 2639.

[54] Abo-Neima, SE, Motaweh, HA, Elsehly, EM. Antimicrobial activity of functionalised carbon nanotubes against pathogenic microorganisms. IET Nanobiotechnology, 14 (2020) 457-64.

[55] Díez-Pascual, AM. State of the art in the antibacterial and antiviral applications of carbon-based polymeric nanocomposites. International Journal of Molecular Sciences, 22 (2021) 10511.

[56] Rogala-Wielgus, D, Zieliński, A. Preparation and properties of composite coatings, based on carbon nanotubes, for medical applications. Carbon Letters, (2023)

[57] Hadidi, N, Mohebbi M. Anti-infective and toxicity properties of carbon-based materials: Graphene and functionalized carbon nanotubes. Microorganisms, 10 (2022) 2439.

View Article Online
DOI: 10.1039/D4NR02810D

View Article Online
DOI: 10.1039/D4NR02810D

DATA AVAILABILITY Some of the data supporting this article have been included as part of the Supplementary Information. All data can be made available upon request to the corresponding author (Emmanuel.flahaut@univ-tlse3.fr).